Sudden Stratospheric Warmings as Catastrophes*

WINSTON C. CHAO

Atmospheric Chemistry and Dynamics Branch, Laboratory for Atmospheres, NASA/Goddard Space Flight Center, Greenbelt, MD 20771

(Manuscript received 22 October 1984, in final form 12 March 1985)

ABSTRACT

In this conceptual and numerical study, sudden stratospheric warmings (SSW) are identified as catastrophes. A catastrophe is the transition toward a separate new equilibrium after the original stable equilibrium state of a dynamical system terminates as an external parameter changes smoothly and slowly across a critical value. Many qualitative results of some previous modeling studies of SSW are interpreted in light of catastrophe theory. For example, the cutoff amplitudes in wave forcing as functions of initial conditions determined by Holton and Dunkerton are shown to be in the loci of unstable equilibria in a bifurcation diagram. Also the stage of warmest polar temperature represents the peak of the overshooting in a catastrophe. Moreover, the rapid restoration of westerlies corresponds to the return from the overshooting. Basic concepts in catastrophe theory related to SSW—for example, hysteresis, cusp and triggering—are demonstrated in a numerical study using the Holton–Mass model.

The transition from the steady regime to the vacillation regime in the Holton–Mass model, i.e., SSW, is explained conceptually in terms of the topographically induced Rossby wave instability. The multiple equilibria involved owe their existence to the resonant response of the system to bottom forcing. The suddenness of SSW is due to the resonant increase of wave amplitude and its positive feedback on the mean flow. The model, as well as the conceptual explanation, gives a resonant buildup of the planetary wave, followed quickly by its decay and then by the warming peak, a scenario corresponding well with observations. A surge of wave amplitude at upper tropospheric levels prior to the warming peak is a result of the instability and, as such, should not be used as a trigger to instigate SSW as in many previous mechanistic models.

Implications of the catastrophic nature of SSW for simulation and forecasting efforts are discussed. An additional and perhaps more difficult challenge in the SSW forecasting effort comes when the initial planetary wave amplitude is not yet in the rapid building-up phase; i.e., before the instability occurs.

1. Introduction

Sudden stratospheric warmings (SSW), the most spectacular dynamical phenomena in the winter stratosphere, have attracted researchers' attention ever since their discovery in the 1950s. Reviews include Quiroz *et al.* (1975), McInturff (1978), Schoeberl (1978), Holton (1980) and McIntyre (1982). In a numerical study, Matsuno (1971) first proposed that SSW are a result of stratospheric mean flow interaction with upward propagating planetary waves originating in the troposphere. His basic idea of wave-mean flow interaction has been reasonably successful in simulating SSW in other mechanistic model studies (e.g., Holton, 1976; Schoeberl and Strobel, 1980). However, his emphasis on the critical line has proved to have been misplaced.

Many global models have also simulated spontaneous SSW (e.g., Grose and Haggard, 1981; Lordi *et al.*, 1980; Mahlman and Umscheid, 1984). Predictions of SSW using general circulation models (GCM) starting from observed initial conditions have been at least qualitatively successful (e.g., Miyakoda *et al.*, 1970; Simmons and Strüfing, 1983; Geller *et al.*, 1985). These studies, along with various observational studies (e.g., O'Neill and Taylor, 1979; Palmer, 1981), have elucidated the evolutionary process of SSW, but the basic theoretical understanding as to why SSW occur and occur so suddenly is not complete. Sudden stratospheric warmings (SSW) often are preceded by a surge in the upward planetary wave flux from the troposphere. Many authors have believed this surge to be a trigger. Is this belief correct? If so, why can SSW be triggered and if not, why? These are among the many unanswered questions.

Attempts to attribute SSW to either barotropic or baroclinic instability have not been fruitful. Recently, Plumb (1981b) suggested that SSW arise from an intrinsic instability of the winter atmosphere in the presence of steady bottom wave forcing. In this instability mechanism, the stationary forced wave acts as a catalyst for the free wave to draw energy from the basic flow. This instability is essentially the topographically induced instability of Rossby waves (Charney and DeVore, 1979; Plumb, 1981a; Pedlosky, 1983; Revell and Hoskins, 1984; Buzzi *et al.*, 1984) and offers some understanding of the SSW process. In this paper this

* Contribution No. 21 of the Stratospheric General Circulation with Chemistry Modeling Project, NASA/GSFC.

instability is investigated from a different perspective. Here we take a conceptual and numerical approach, guided by catastrophe theory, in obtaining some qualitative understanding of SSW.

Using a severely truncated quasi-geostrophic β-plane model, Holton and Mass (1976; hereafter HM) showed that the model stratosphere exhibits recurrent warmings when the steady wave forcing at the bottom boundary exceeds a critical value. When the forcing is subcritical, the model stratosphere reaches a steady equilibrium close to the radiative equilibrium. The equilibrium—or quasi-equilibrium—state on the other side of the critical forcing has a completely different structure (see Fig. 1 of HM). The sudden cessation of a final equilibrium solution and the appearance of another totally different one, as an external parameter is changed slightly, is reminiscent of a catastrophe.

Catastrophe theory, a branch of the combined fields of calculus, differential equations and topology, was first systematically elaborated by Thom (1972), and has subsequently been applied to atmospheric sciences. It has been used in studies of Rayleigh–Benard convection, quasi-geostrophic flows, climate and the onset of turbulence (see Dutton, 1982 and the bibliography therein). Because the nomenclature is not unified, this theory has also been termed—or overlaps with—bifurcation theory, structural instability, singularity theory, etc. For an introduction to catastrophe theory, refer to Poston and Stewart (1978), Saunders (1980), and Arnold (1984).

A simple example of a catastrophe taken from nonlinear dynamics is given in Section 2 to illustrate some basics of catastrophe theory. Readers who are already familiar with the theory may find this section elementary. In Section 3, many qualitative results from previous modeling studies of SSW are interpreted in light of catastrophe theory. Further properties of this theory essential to SSW such as hysteresis, cusp and triggering are demonstrated in a numerical study using the HM model in Section 4. A qualitative explanation of the transition from the steady regime to the vacillation regime in the HM model in terms of the topographically induced barotropic Rossby wave instability is offered in Section 5. Some implications for simulation and prediction of SSW are discussed in the final section.

2. Some basic concepts in catastrophe theory

A simple example depicting a catastrophe is Benjamin's buckling of a wire arch under gravity (Iooss and Joseph, 1980). His apparatus (Fig. 1) is a board with two holes through which a bicycle brake cable is passed. The length of the wire above the board, l, an independent variable, can be adjusted slowly and continuously by moving one end of the wire. The equilibrium state of the wire is denoted by the angle θ, a dependent variable. When l is small, the only equilibrium state is the upright one ($\theta = 0$). This upright state remains as l is increased *slowly* until l exceeds a critical value l_c. At that instant, θ changes abruptly to a finite value, either positive or negative, representing a right or left bend. Further increasing l results in a continuous change in θ. On the other hand, when l is decreased past l_c, θ does not change abruptly back to zero; instead, it decreases continuously until another critical l, l_0, is reached, when θ snaps back to zero.

Figure 2 shows the bifurcation diagram where stable equilibrium states are drawn in solid lines and unstable equilibrium states in dashed lines. The dashed lines indicate mathematically possible, but physically unrealizable, equilibrium states. The abrupt loss of stability of an equilibrium solution as an external parameter slowly passes a critical value and the simultaneous racing towards another equilibrium solution is called

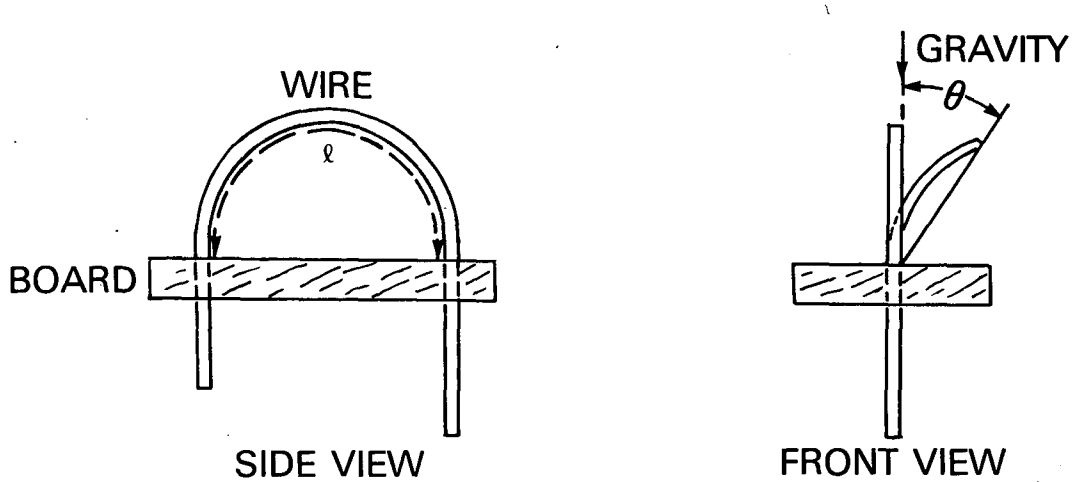

FIG. 1. Front and side view of Benjamin's wire arch which contains a board with two holes through which a bicycle brake cable is passed. The state variable is the inclination angle θ, and the external adjustable parameter is the wire length l above the board. (Courtesy of Iooss and Joseph, 1980)

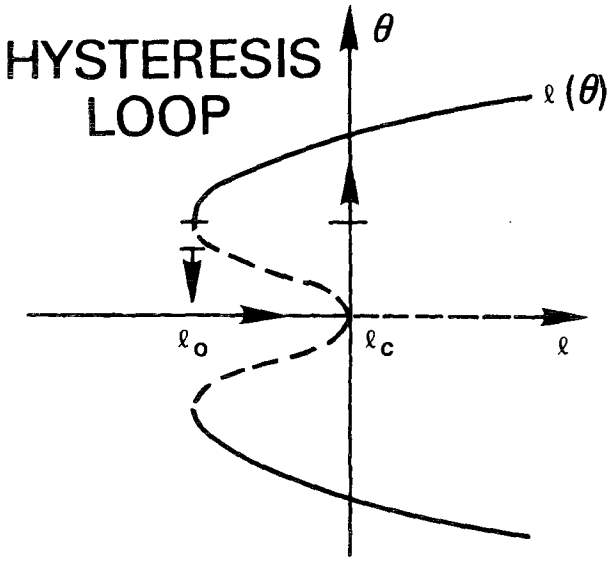

FIG. 2. Bifurcation diagram of the wire arch experiment, which shows the stable (solid) and unstable (dashed) equilibrium states as functions of wire length l. (Courtesy of Iooss and Joseph, 1980)

a catastrophe. In the range between l_0 and l_c, there are three stable equilibrium states, and the choice depends on the past history of the system. This phenomenon is called hysteresis.

The loci of the solid lines can be determined experimentally as described above. Those of the dashed lines can also be determined experimentally. If an experiment is done with a fixed l ($l > l_0$), by holding θ at an arbitrary initial value θ_i and letting go, i.e., $(d\theta/dt)_i = 0$, then which equilibrium state θ will come to rest at depends of course on θ_i. In a series of experiments with successively increasing θ_i, there is a critical θ_i, $\hat{\theta}_i$, across which the final θ will reside on different solid lines. By repeating this series with different l's, one obtains $\hat{\theta}_i$ as a function of l, which is the locus of the dashed lines. This series of experiments can also be done in an inverse manner by using the same θ_i and successively increasing l, and thus obtaining a critical l, $\hat{l}$. By repeating such a series of experiments with different θ_i's, one gets the same loci. In more general cases with nonzero initial $d\theta/dt$ and θ_i, when similar experiments are done, one can obtain instead of the dashed lines, "dashed" surfaces in the 3-D space of θ, $d\theta/dt$ and l, which of course intersect the θ–l plane at the dashed lines in Fig. 2.

The values of l_0 and l_c depend on the stiffness, or elasticity, of the wire. Figure 3 shows a schematic diagram of this dependence in a cusp shape. The bifurcation diagram also depends on the stiffness. If the stiffness is very great, only the upright state of equilibrium can exist. On the other extreme, if the degree of stiffness is very low, only the bent state can exist. In the intermediate range, the bifurcation diagrams are of two different types, depending on the physical properties of the wire such as stiffness and weight per unit length (Fig. 4). In Type A, the solid lines are connected; thus, the transition from one branch of the equilibrium to another involves continuous, noncatastrophic and nonexplosive changes of states. In Type B, on the other hand, the solid lines are disconnected and the transition is discontinuous, catastrophic and explosive (Sturrock, 1966). Type A is often referred to as a bifurcation and Type B as a catastrophe.

It is essential to recognize that catastrophes can be triggered. When $l_0 < l < l_c$, if the system in a nonbent state ($\theta = 0$) is subject to a sufficiently large outside disturbance in the form of a shaking motion and/or a jerking push or pull of one end of the wire, θ will move into one of the other regions separated by the "dashed" surfaces in the 3-D space of l, θ and $d\theta/dt$, ("*surfaces* of no return"), and θ will start racing toward one of the other equilibria. The required intensity of the trigger is, of course, a function of how far the current equilibrium state is away from the "dashed" surfaces. The triggering process may proceed at any speed, but the catastrophe usually proceeds quickly once under way. Exactly how sudden the catastrophe is largely depends on the physical properties (e.g., the stiffness) of the wire, though the intensity of the trigger is also a determining factor.

The entire picture can also be viewed by considering the potential energy (sum of the gravitational and the elastic potentials) distribution. Figure 5 shows the potential energy as a function of θ for different l's. The location of the particle represents the state of the system. When $l = l_2$, the particle at equilibrium can be pushed (or triggered) over the potential energy peak, falling into the neighboring valley (a triggered catastrophe). Alternatively, when l is increased beyond l_c, a spontaneous catastrophe occurs. How fast the particle falls naturally depends on the steepness of the walls of the valley and the intensity of the push in a triggered catastrophe. If the dissipation is not too great, the falling particle will overshoot the new stable equilibrium position and oscillate about it a number of times before coming to rest.

The sequence of pictures can also be viewed in a reverse order, with decreasing l. Starting from $l > l_c$, the particle lies in either of the two valleys. As l decreases, a new valley develops at the center, but the particle remains in the original valley until $l < l_0$, and the particle falls into the central valley as the side valleys disappear. Thus, when $l_0 < l < l_c$, the particle may be found in any of the three valleys, depending on its past history (i.e., hysteresis). Also the shape of the potential energy distribution shows multiple equilibria. If the stiffness of the wire is such that the bifurcation diagram is of Type A, then as l increases, instead of the appearance of two humps on either side of the particle in the energy diagram, a single hump develops at the center. In this instance, the particle moves slowly as the valleys deepen and no catastrophe occurs.

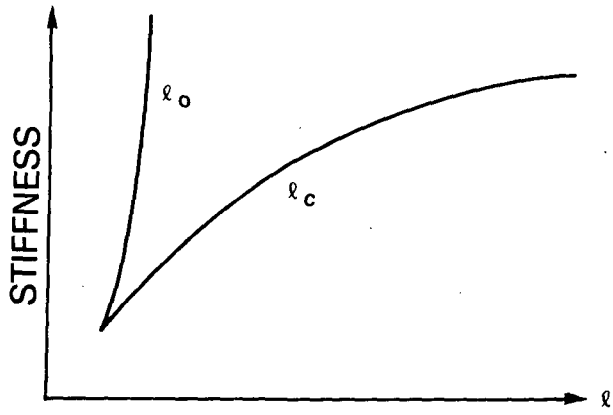

FIG. 3. Schematic diagram of the cusp dependence of l_c and l_0 on physical properties of the wire such as stiffness and weight per unit length.

In a more general system with more degrees of freedom and with an energy source, sink and/or other instability mechanisms, the equilibrium states can have different characteristics; i.e., they can be steady (fixed point), time-periodic (limit cycle) or time aperiodic (quasi-equilibrium, attractor set or strange attractor). For example, the transition between wavenumber regimes in annulus experiments, a catastrophe whose suddenness and hysteretic nature have been clearly demonstrated (Fultz *et al.*, 1959), involves two time-periodic equilibria. Often the two equilibria involved in the change have different characteristics. For instance, the transition from the Hadley regime to the Rossby regime in annulus experiments, also a catastrophe, involves steady and time periodic equilibria.

3. Interpretation of some previous modeling results of SSW

Although the proof that SSW is a catastrophe will not be forthcoming until the numerical study in Section 4 is presented, one can interpret many of HM and Holton and Dunkerton's (1978; hereafter HD) model results, along with some observational results, assuming such a hypothesis is valid. These interpretations will also help to design further model experiments to verify our assumption. Before doing so, however, a recapitulation of HM and HD is useful.

Holton and Mass studied the wave-mean flow interaction in the stratosphere using a quasi-geostrophic, β-plane channel numerical model, an outgrowth of Geisler's (1974) model. This model extends vertically from 10 to 80 km, and over 60° in the meridional domain. In the zonal direction, only one wavenumber is allowed, and in the meridional direction, only one mode exists. In the vertical direction, the model has a 2.5-km size grid system. External forcings include latitudinal differential heating, parameterized in terms of Newtonian cooling, and a steady bottom boundary wave forcing. The zonal wind at the bottom is fixed. The initial conditions correspond to a zonally symmetric flow closely resembling the winter mean conditions in the Northern Hemisphere.

Holton and Mass did a series of experiments starting from the same initial conditions, but with different bottom wave forcing amplitude rising in three days and staying constant thereafter, and studied the resulting equilibrium (or quasi-equilibrium) state. They found that when the bottom forcing is sufficiently small, the model's final state is a steady circulation very close to radiative equilibrium conditions. However, when the amplitude of the steady bottom boundary wave forcing h_B (as defined in Eq. (11) of HM) exceeds a critical value $\hat{h}_B$ the final state is no longer steady; instead, the mean zonal flow and eddy components oscillate quasi-periodically; i.e., the model exhibits repeated warmings, or vacillation. With the exception of the first one, these repeated warmings do not show any suddenness. Also, the time mean of the vacillation solution is very different from the radiative equilibrium state.

Holton and Mass concluded that oscillation in stratospheric long waves does not necessarily reflect oscillating tropospheric forcing, but may occur even in the presence of steady bottom forcing. This conclusion is not particularly surprising, since vacillation has been known to exist under steady external forcing parameters in annulus experiments. (It should be stressed that steady external forcing parameters can still allow nonsteady external forcings. In the HM model, the radiative forcing is nonsteady.) However, this finding is significant since it demonstrates the importance of the internal nonlinear dynamical processes associated with stratospheric planetary waves.

Subsequently, HD continued the same study and showed that wave transience, not dissipation, is the primary mechanism for generating mean flow oscillation. In addition, in a series of experiments, they found that the critical wave forcing amplitude necessary to produce a vacillation response is very sensitive to the initial mean flow profile, which in their experiments is identical to the radiative equilibrium profile.

The relevance of HM and HD's results to the real stratosphere is supported by another β-plane model (Schoeberl, 1983) which has more degrees of freedom in the meridional direction and has demonstrated similar critical bottom wave forcing amplitude.

If an analogy is drawn between HM and HD's experiments and the buckling of the wire arch example in Section 2, one can identify h_B with l, the model state—a point in a multidimensional phase space—with θ, and the vertical gradient of radiative equilibrium zonal wind, $\partial U_R/\partial z$, with the stiffness. The model bifurcation diagram looks conceptually like that in Fig. 6. (Fig. 6 may or may not be a complete picture, since there might be other equilibrium states not found in

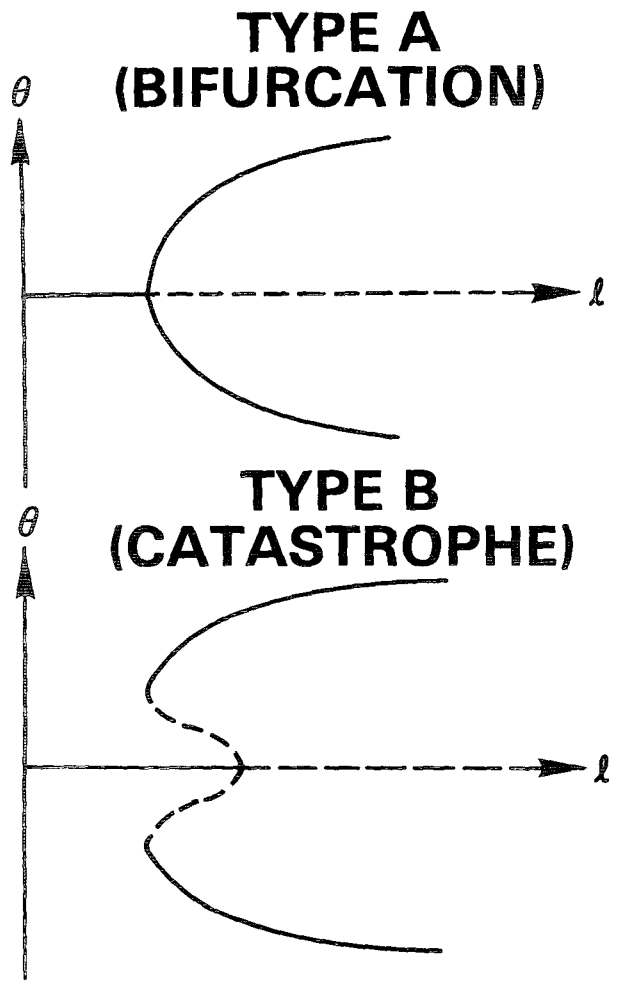

FIG. 4. Types A and B bifurcation diagrams. Stable equilibria (solid lines); unstable ones (dashed).

HM and HD's experiments. Indeed, as shown later, it is incomplete.) The upper solid line represents the vacillation regime and lower one, the steady regime. The dashed line represents the unstable equilibrium states or the loci of the "potential energy hump." The warmings they obtained correspond to the phase of the vacillation that is farthest from the steady regime. The first few warmings in the model have the help of overshooting. (The first occurrence of overshooting in the valley brings the particle farthest from the new equilibrium. Likewise, the first warming in HM's results is the strongest.)

The experiments done by HM and HD in finding the critical bottom forcing amplitude are analogous to the series of experiments on the buckling wire arch described in Section 2 in searching for $\hat{l}$ as a function of θ_i, or more precisely, for the "dashed" surface in the 3-D space of l, θ_i and $(d\theta/dt)_i$. From this analogy, it is not surprising that HD's results showed that $\hat{h}_B$ depends on the initial conditions [since $\hat{l}$ is a function of θ_i and $(d\theta/dt)_i$, $\hat{h}_B$ is equivalent to $\hat{l}$, or more precisely, to a point on the "dashed" surface, rather than to l_c]. Furthermore, the fact that this dependence is very sensitive to the initial conditions only indicates that $(h_B)_0$, corresponding to l_0, and $(h_B)_c$, corresponding to l_c, are far apart. For the sake of discussion we have ignored the fact that h_B was gradually turned on in three days in HM and we assume that h_B is turned on instantly. Parenthetically, in HD, for different experiments with a fixed bottom zonal wind, $\partial U_R/\partial z$ was changed, but this does not affect our conclusion.

To find the critical amplitude of the bottom boundary forcing $(h_B)_c$ corresponding to l_c, one needs to start from an equilibrium state—a final state in HM's experiments with small h_B—and integrate with time, with a very gradual increase of h_B, so as to keep the model state in equilibrium. Eventually when h_B increases past $(h_B)_c$, the model will jump into the vacillation regime within a short time, i.e., a catastrophe or SSW will occur. Similarly, to find the h_B corresponding to l_0, $(h_B)_0$, one should start from a vacillation state and decrease h_B gradually; these experiments have been done (see Section 4).

Though there is a fundamental analogy between the wire arch and HM's model, a number of differences

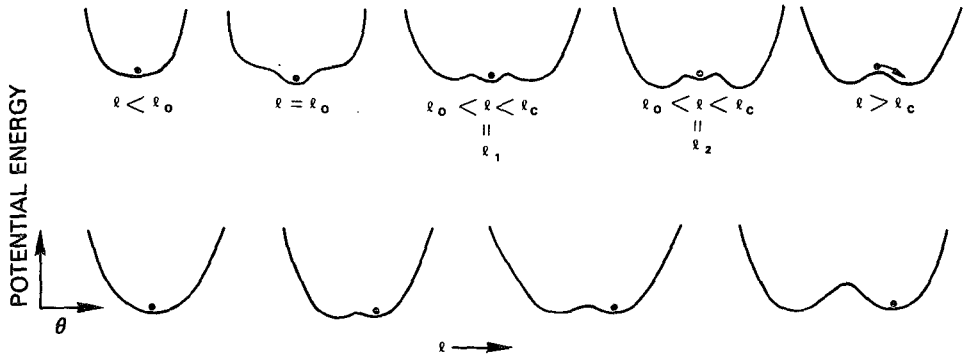

FIG. 5. Potential energy distribution as a function of θ for various l's. Upper part for Type B; lower part for Type A.

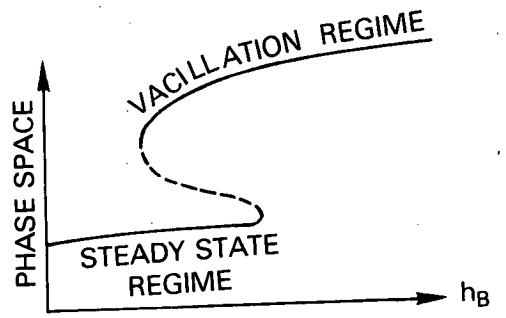

FIG. 6. Schematic diagram showing the two stable equilibrium regimes (solid) and unstable ones (dashed) in the HM model.

exist between them that arise from the greater number of degrees of freedom and the existence of external forcings in the HM model. The oscillation of the particle in the potential energy valley in the wire arch experiment involves only exchange of kinetic energy and potential energy, whereas the vacillation in the HM model involves the additional, and more important, energy exchange between wave and zonal flow. In the wire arch example, the particle periodically passes through the bottom of the potential energy valley before coming to a rest. In the HM model, the state particle may spiral toward the valley bottom, and the valley bottom is not necessarily a point in a N-dimensional state space and can occupy a space of up to $N - 1$ degrees of freedom.

For the particle representing the state of the wire arch to continue oscillating in the potential energy valley (Fig. 5), it has to experience an external time dependent forcing. Similarly, in the vacillation regime, the model experiences time dependent radiative forcing; thus, time dependent bottom boundary forcing is not necessary. However, in the model, the time period, regular or irregular, of the radiative forcing and of the vacillation itself is internally determined, whereas the time period of the particle oscillation can be completely determined externally. If the bottom forcing is oscillatory, then the model should have an additional oscillation with the same frequency. Still more frequencies may appear also, due to nonlinearity and/or other instability mechanisms, if more degrees of freedom are introduced into the model.

Observations show that SSW is often preceded by a surge of upward wave energy flux from the troposphere. Many authors believe that this surge acts as a trigger for SSW. This belief may fit the description of SSW as a catastrophe, which by definition can be triggered, and is tested in a numerical study in Section 4. The rapid restoration of the westerlies after a warming resembles the return of the overshot particle in the potential valley towards the new equilibrium state. As just mentioned, the steady state equilibrium for $h_B < (h_B)_c$ in HM's result can be generalized to allow vacillation—a vacillation of much smaller amplitude that does not result in warmings—either by imposing a periodicity on the bottom boundary wave forcing as the index cycles in the troposphere might suggest, and/or by allowing more zonal wavenumbers (or meridional modes) to interact nonlinearly with each other and with the zonal mean flow. The results would resemble the vacillation observed in the stratosphere with a quasi-two-week period (Hirota and Sato, 1969) before any warming event takes place.

4. Numerical experiments using the HM model

The model used is that of HM; a very brief description of it is given in Section 3. Their parameter settings, along with their notations, are strictly adhered to unless otherwise specified. The code was written exactly as documented in HM. As stated in HM, all results from this model should be considered as *heuristic* only, because the quantitative details are certainly affected by the severe truncation and because sphericity is not taken into account. Results for wavenumber 2 will be discussed first.

a. Spontaneous SSW

The initial conditions used are those of HM: a 10 m s^{-1} bottom zonal wind, a constant vertical zonal wind shear of 3 m s^{-1}/km up to 50 km, and zero shear above it at midchannel. At the model top both the wave amplitude and the mean wind are set at zero. The radiative forcing gives a vertical shear of the radiative equilibrium zonal wind, $\partial U_R/\partial z$, of 3 m s^{-1}/km, which corresponds to the winter solstice condition. The bottom boundary (at 10 km) steady wave forcing of wavenumber 2 has an amplitude of $h_B = 40$ m, rising in three days. (Note that the amplitude of bottom forcing is $h_B \exp(z_B/H) \approx 2h_B$, where z_B is the model bottom height and H is the scale height. See Eq. 7a of HM.) Then h_B was increased by 0.075 m day^{-1} as the integration continued until termination at day 2000. Figure 7 shows the transition from a near radiative equilibrium state to a (quasi-) periodic vacillation state of repeated warmings at approximately day 1600 when $h_B \approx 159$ m, denoted by $(h_B)_c$. The repeated warmings follow the first warming as shown in the figure. The near barotropic nature of the transition is indicated by the nearly vertical phase contours in Fig. 7c. The transition occurs almost simultaneously at all levels. Before the transition, the wave has only a very small vertical phase tilt and is essentially in phase with the topography. The model SSW is characterized by an anomalous increase in wave amplitude, followed by a rapid decay. The wave phase shows a westward movement. In the meantime, the zonal wind decreases ever more rapidly and becomes zero just as the wave amplitude peaks. The zonal wind then continues its decrease at a progressively slower rate and soon reaches a peak easterly, which represents the peak of the warming.

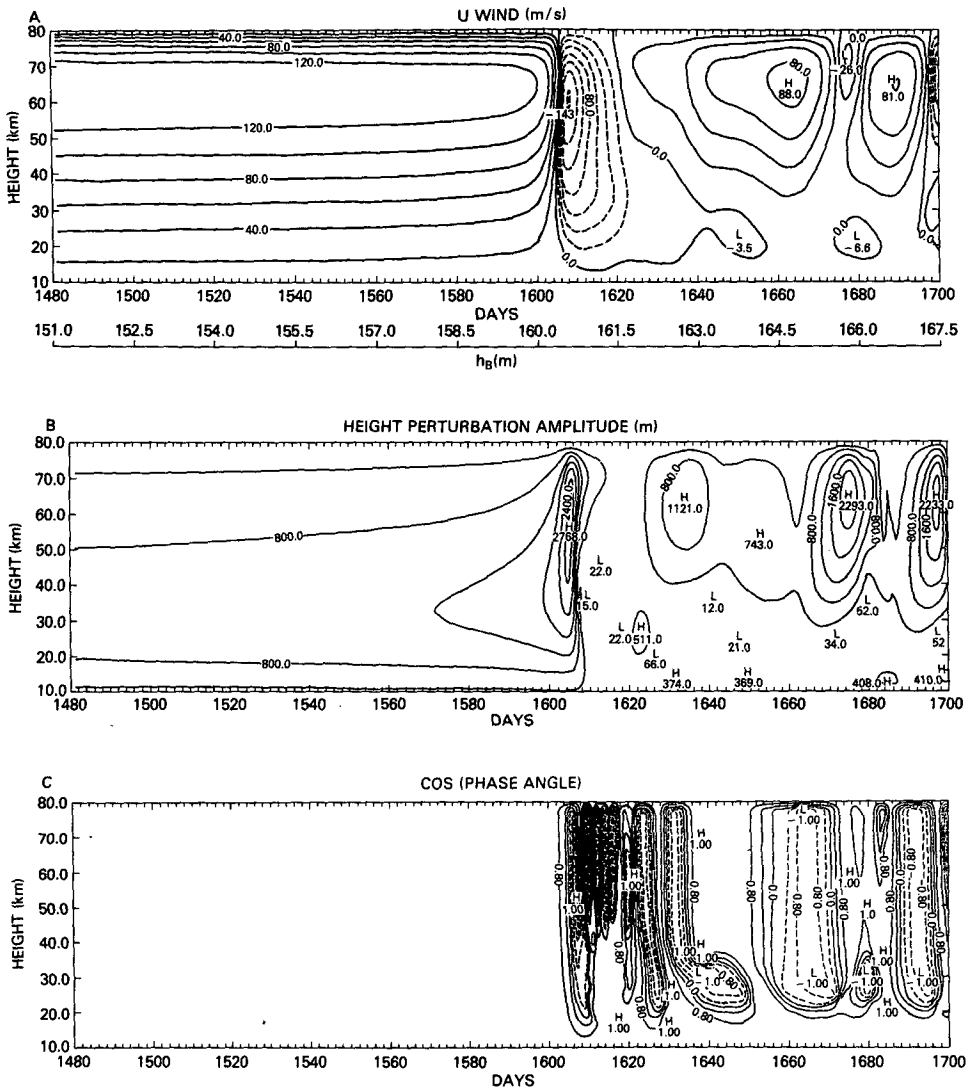

FIG. 7. Spontaneous SSW for wavenumber 2, $\partial U_R/\partial z$ = 3 m s^{-1}/km, U_B = 10 m s^{-1}; (a) time-height section of zonal mean wind (m s^{-1}) at midchannel; (b) height perturbation amplitude (m); (c) cosine of phase angle; Note: h_B was raised from 40 m at a rate of 0.075 m day^{-1}.

Figure 8 shows a more detailed picture of the evolution at 40 km. The subsequent restoration of the westerly is also very rapid. The sequence of events exhibits a good resemblance to real warmings.

b. *Hysteresis and cusp*

To find $(h_B)_0$, an experiment was started from h_B = 70 m rising in three days, which is sufficient to put the model state in the vacillation regime; h_B was then reduced at a rate of 0.025 m a day. The transition from a vacillation regime to a steady state regime occurs almost simultaneously at all levels when $h_B \approx 26.5$ m (Fig. 9). This transition is much slower than the one reported in Section 4a, though it shows the same barotropic nature. Since $(h_B)_c > (h_B)_0$, there is a range of h_B values where both flow regimes can coexist. Thus, the hysteretic property of the model is established, and the catastrophic nature of the sudden warmings in the model is identified.

In an attempt to obtain the dependence of $(h_B)_c$ and $(h_B)_0$ on $\partial U_R/\partial z$, the two experiments described above were repeated with $\partial U_R/\partial z$ equal to 2 m s^{-1}/km and then 1 m s^{-1}/km. The experiments with increasing h_B to obtain $(h_B)_c$ gave qualitatively similar results. However, the experiment with decreasing h_B starting from the vacillation regime and with $\partial U_R/\partial z$ = 1 m s^{-1}/km showed two consecutive transitions. The first is a transition from the vacillation regime to a steady state regime; this is different from the steady state we have found in the early experiments before the warming occurs in that the wave is baroclinic and the state resem-

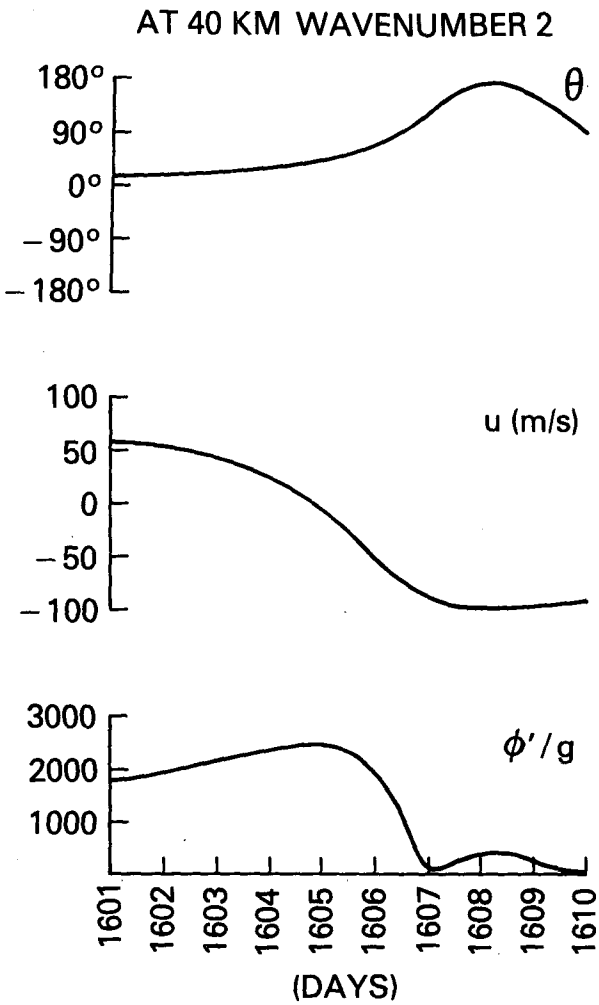

FIG. 8. Detailed evolution of model SSW (shown in Fig. 7) at 40 km.

bles closely the time mean of the vacillation regime. This transition occurs first at lower levels and then spreads into higher levels in about four hundred days. The second transition brings the state to a steady state similar to that found before the warming in the earlier experiments, i.e., the wave is in phase with respect to the bottom forcing. In the second transition the wave is coherent in height. Upon reexamination of the results from similar experiments for $\partial U_R/\partial z = 3$ m s^{-1}/km and $\partial U_R/\partial z = 2$ m s^{-1}/km cases, hint of the first transition was found though the second transition is more readily identified. Figure 10 shows the dependence of $(h_B)_c$ and $(h_B)_0$ on $\partial U_R/\partial z$ in a cusp form. Curve $(h_B)_0$ corresponds to the transition into the near radiative equilibrium solution. The first transition in the decreasing h_B cases occurs fairly close to $(h_B)_0$ and is not shown in Fig. 10. When the state of the external parameters moves into the region flanked by the two curves, nothing drastic happens. On the other hand, when the state of the external parameters continues moving in the same direction and leaves the shaded region, a catastrophe occurs. (On leaving the region on the $(h_B)_0$ side, two consecutive transitions occur.)

In other experiments with wavenumber 2, it was found that $(h_B)_c$ and $(h_B)_0$ both decrease as the specified bottom (at 10 km) zonal wind U_B is decreased. This is consistent with HD's finding (Table 1 of HD) that $\hat{h}_B$ decreases with U_B (at the surface).

c. *Triggering*

To demonstrate that SSW can be triggered, an experiment was done with wavenumber 2, $\partial U_R/\partial z = 3$ m s^{-1}/km, and with h_B slowly increasing from 0 to 140 m, which is below $(h_B)_c$, in 1000 days, and kept at 140 m from day 1000 to day 1600. At day 1600, h_B was raised abruptly to 160 m, and it remained at that value for 10 days (shorter than the radiative relaxation time scale in the lower portion of the model), and was then restored to 140 m. Computation was continued until day 2000. Figure 11 shows the evolution of zonal winds and reveals a sudden jump from a steady equilibrium state to a vacillation, as a result of the triggering. When the same experiment was repeated with the raised value of h_B, 160 m, replaced by 150 m, starting on day 1600, the model state experienced only a slight perturbation and no sudden warming, and it soon returned to the original near-radiative equilibrium state. These results fit perfectly with the triggering concepts discussed in Section 2. Perturbation in external parameters or in boundary condition parameters other than h_B can also serve as a trigger, as can nonlinear wave–wave interaction which is present in a more complete model. Moreover, perturbing prognostic quantities in the model can also trigger SSW.

d. *Wavenumber 1 results*

An experiment was done with the same initial condition as before, with h_B increasing from zero at a slow rate, and with wavenumber 1. For small h_B, the steady state wave is almost barotropic and exhibits a nearly 180° out-of-phase relationship with respect to bottom forcing; transition to the vacillation regime first occurs at higher levels and then spreads slowly downward (Fig. 12). Such a slow transition bears no resemblance to real warmings and is clearly different from the transition discussed in Section 4a. The hysteretic nature of the wavenumber 1 transition is revealed in Fig. 13, which shows two steady equilibrium states at the same bottom forcing amplitude. The steady equilibrium, (a) in Fig. 13, is the near radiative equilibrium state before the transition that exhibits the nearly 180° out-of-phase relationship with respect to bottom forcing, and is distinguished from the steady state obtained by HM. Solution (b) is the low forcing limit of the vacillation regime and is obtained by starting from vacillation solution and reducing bottom forcing. In the vacillation regime, the period of vacillation becomes greater as h_B decreases (Fig. 5 of HM). The period of vacillation becomes infinity, i.e., a steady state, as $h_B < 60$ m. Schoe-

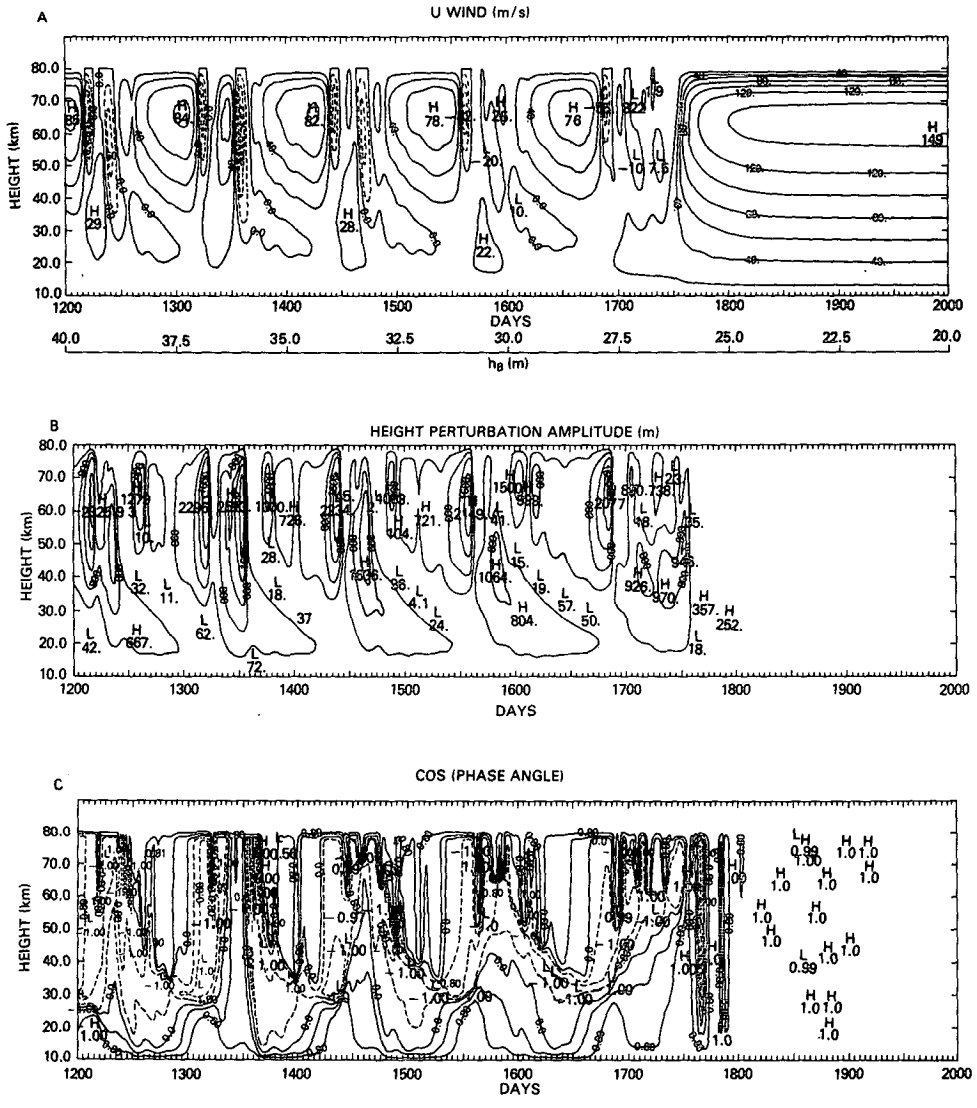

FIG. 9. As in Fig. 7 except for decrease of h_B from 70 m at a rate of 0.025 m day^{-1}.

berl (1983) also found a steady solution similar to (b) in an extended model, and attributed its existence to the fact that his model allows more meridional modes which facilitate the critical level's turning reflective. The current study shows, in contrast, that this steady state is a low forcing limit of the vacillation regime, and can exist even when only one meridional mode is allowed in the model. The cusp for this transition is difficult to obtain, since the two critical curves forming the cusp are very close to each other.

e. Comparison with Holton–Mass code

Professor Holton kindly provided us with the HM code listing for comparison purposes. Their code had the model bottom at the surface. We failed to follow enough details in their code to move the model bottom to 10 km. After changing the model bottom to surface in our code, we used the two sets of codes to run the spontaneous SSW experiment reported in Section 4a. Both codes gave $(h_B)_c$ of about 330 m and the other quantitative results compared very well. Also, results from their code exhibited the same hysteretic property. However, when our code was used to repeat the experiments reported in HM with bottom forcing rising in three days, the critical h_B we obtained was around 50 m, about one-third of that reported in HM. This discrepancy is hitherto unresolved.

5. A conceptual explanation of the catastrophe in the HM model

Thus far we have only identified through experiments that SSW, at least as appeared in the Holton–Mass model, are catastrophes. The fundamental questions of why SSW occur at all and why so suddenly

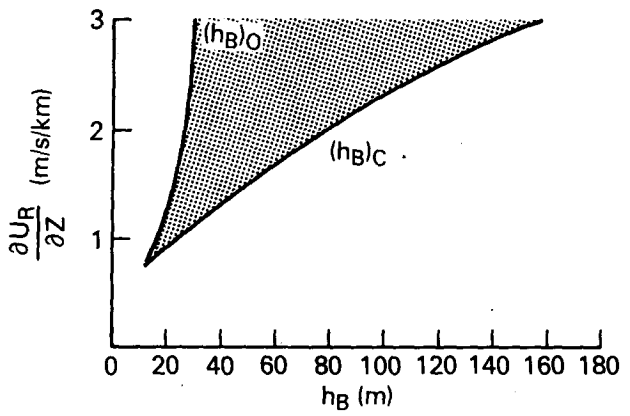

FIG. 10. Cusp dependence of critical bottom wave forcing amplitudes $(h_B)_c$ and $(h_B)_0$ on radiative forcing $\partial U_R/\partial z$ for wavenumber 2.

have not been addressed. The fact that SSW are catastrophes does not explain the suddenness. As discussed earlier, the speed of a catastrophe depends on the slope of the new potential valley wall which in principle can have any value. This section provides answers to these fundamental questions.

An explanation of results of the numerical experiments shown in Section 4 can be obtained by first looking at the topographically induced barotropic Rossby wave instability (TIBI). The TIBI was first investigated by Charney and DeVore (1979; hereafter, CD) in explaining blocking. The multiple equilibria associated with the TIBI were discovered in an earlier independent work by Vickroy and Dutton (1979). The TIBI was subsequently studied and reviewed by many authors. The brief discussion of TIBI in the following paragraph is based on a concise review of CD by Held (1983).

As shown by Held, a β-plane channel shallow water flow (or a divergent barotropic flow) over wavy topography can be described by quasi-geostrophic approximation as:

$$\frac{\partial [u]}{\partial t} = -\kappa([u] - [u_e]) - D([u]) \qquad (1)$$

which states that the zonally averaged zonal wind, $[u]$, in the absence of the drag by steady forced waves generated by topography, $D([u])$, relaxes to an equilibrium value, $[u_e]$, through an external forcing, which in a baroclinic atmosphere would be the radiative forcing. The associated relaxation time scale is κ^{-1}; $D([u])$ is the sum of the eddy momentum flux divergence and the form drag. In a baroclinic model, $[u_e]$ would be the radiative equilibrium zonal mean wind. Held also showed that $D[u]$ is equal to the southward eddy flux of potential vorticity. When the wave consists of only one meridional mode, $D([u])$ has the same shape as $[\eta^{*2}]$, where η^* is the perturbation of surface height and is proportional to the amplitude of bottom topography. The steady state solution of (1) is shown schematically in Fig. 14. The peak of $D([u])$ corresponds to a resonance. If the parameters are such as to produce the graph shown, three equilibria exist. It is clear from Eq. (1) that if $\kappa + dD/d[u]$ is negative, as it is for the intermediate equilibrium, point B, the state is unstable. A physical explanation for the TIBI for the case of $\kappa = 0$ is given by Revell and Hoskins (1984). The equilibrium state "A" corresponds to a high wave amplitude and low zonal wind "blocking state" and the other equilibrium state C corresponds to a low wave amplitude and high zonal wind "normal state." Also, solution C is nearly in phase with the bottom forcing whereas solution A is nearly 180° out-of-phase with the bottom

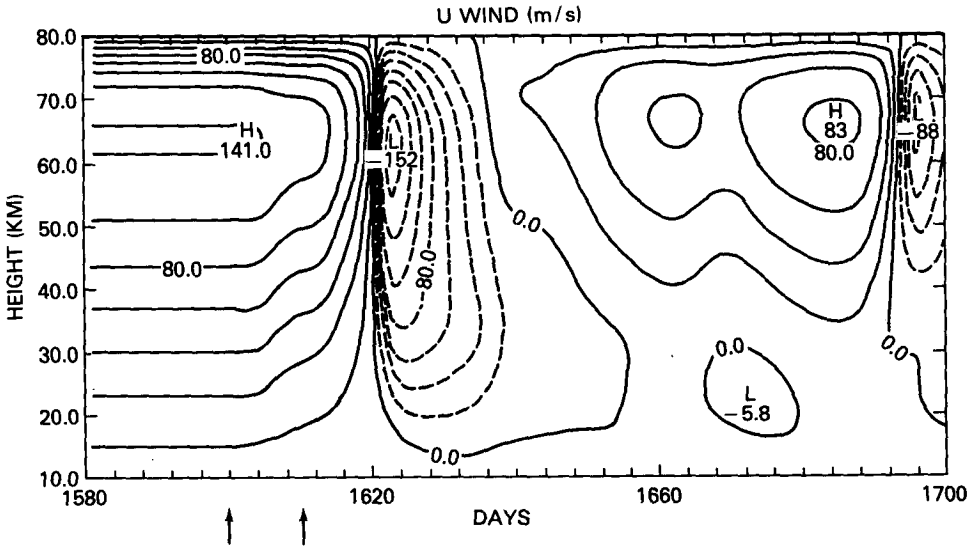

FIG. 11. Time-height section of zonal mean wind at midchannel for wavenumber 2, illustrating the triggering effect; h_B is raised from 140 to 160 m at day 1600 and restored to 140 m at day 1610.

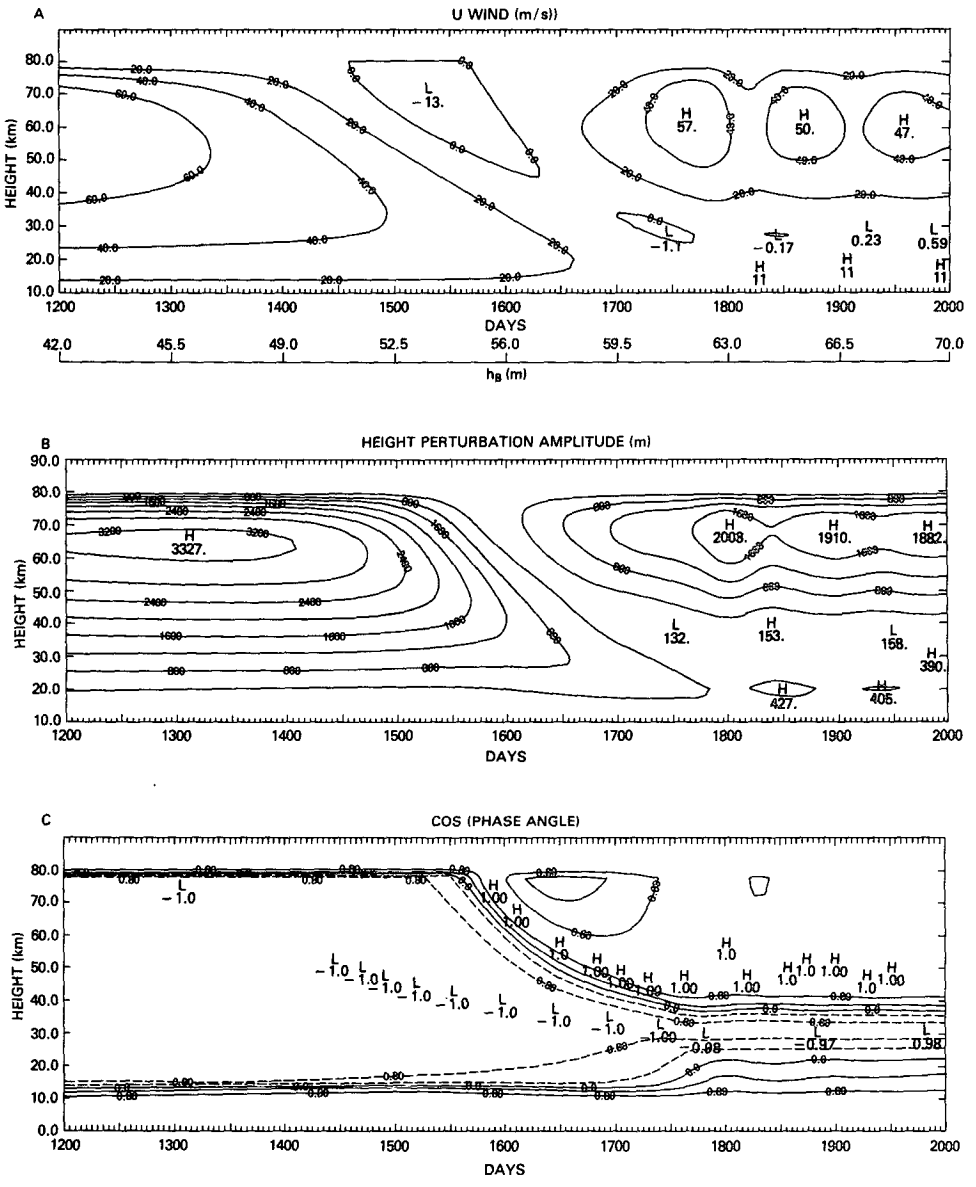

FIG. 12. As in Fig. 7 except for wavenumber 1; h_B was raised from 0 m at a rate of 0.035 m day^{-1}.

forcing. Clearly, the multiple equilibria owe their existence to the resonant structure in $D([u])$.

Equation (1) and Fig. 14 can be used to investigate the HM model, which is identical to the CD system except for its being vertically stratified, in an analogous manner. Steady solutions that exist in a barotropic model have their counterparts in the corresponding baroclinic model. However, a steady solution that is stable in a barotropic model may become unstable as the model is switched to a baroclinic one, due to the additional degree of freedom in the vertical direction in the baroclinic model. The numerical results in Section 4 indicated that in the HM model, solution C remains stable and solution A becomes unstable when the bottom forcing is large. Also, the steady solution A, when unstable in the stratified flow, is replaced by a stable limit cycle (periodic) or attractor (aperiodic).

Before further elaborating on these numerical findings, we would like to note the differences and the analogy between the CD and HM systems. Unlike the shallow water system where the change in bottom wave forcing is felt at all heights simultaneously, the baroclinic atmosphere has to depend on vertical wave propagation for any change in bottom wave forcing to influence higher levels. Also, for lack of thermodynamics, the shallow water system has no meridional heat flux as does the baroclinic atmosphere. Despite these differences, the important point for our explanation of the results in Section 4 is that the HM model also has analogous multiple equilibria; this is borne

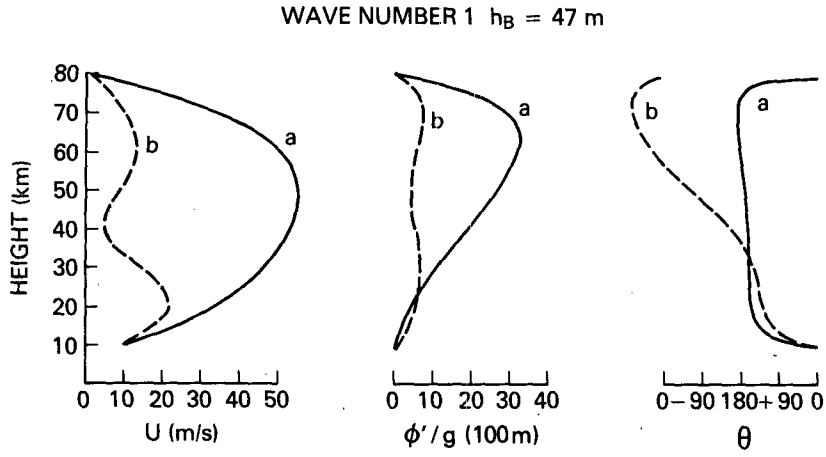

FIG. 13. Two steady state solutions at midchannel for wavenumber 1; h_B = 47 m and $\partial U_R/\partial z$ = 3 (m s^{-1} km^{-1}). Curve (a) is the near radiative equilibrium solution. Curve (b) is a limit solution which bifurcates into a vacillation solution when h_B is increased.

out by the numerical experiments which owe their existence to the resonant structure in the wave forcing of the mean flow.

The steady equilibrium solution in the HM model is a counterpart of solution C of the CD system, which is close to the radiative equilibrium state. This identification is clear from Fig. 7 which shows the evolution of phase and amplitude of the wave disturbance and the zonal flow speed in the HM model as the amplitude of the bottom wave forcing gradually increases. Before the warming occurs, the equilibrium steady state exhibits an almost barotropic structure forced by bottom topography. This almost barotropic structure materializes because of a low reflecting level, above which the wave is evanescent and below which the upward propagating wave combines with the reflected downward propagating wave to give the almost barotropic structure. The stationary wave is almost in phase with the topography; the minute out-of-phase feature exists in response to the dissipation in the model, which is greater at higher levels. When h_B is very small, the peak of $D([u])$ is lower than $\kappa([u] - [u_e])$ and the solutions A and B do not exist. Solution C is the only solution. As the topographic amplitude increases, the curve $D([u])$ in Fig. 14 moves upward and solutions A and B appear but the model solution is still at point C. As the topographic amplitude continues increasing, point C moves upward and point B moves downward at a

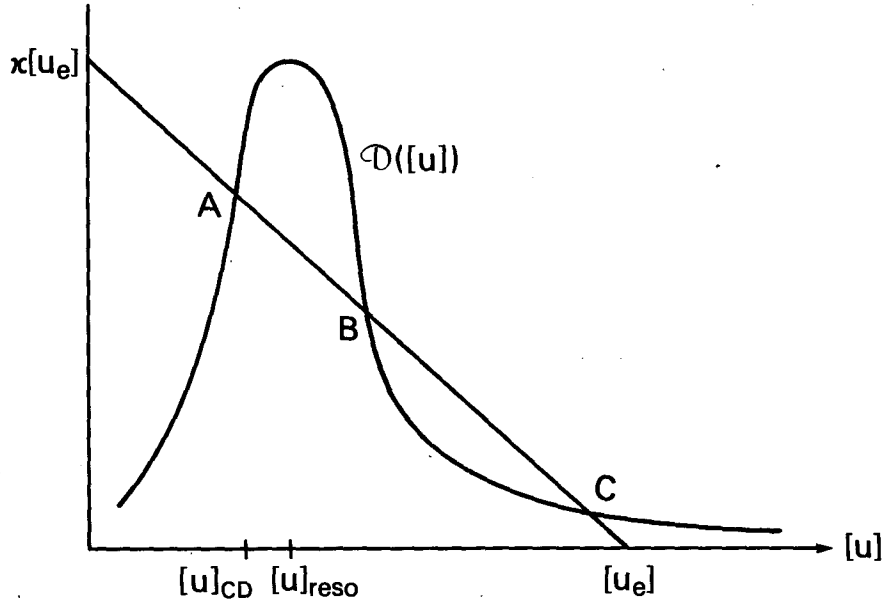

FIG. 14. Schematic representation of Eq. (1). (Adapted from Held, 1983)

slower rate along the line $\kappa([u] - [u_e])$. Similarly, in the HM model the steady solution experiences a gradual decrease in zonal flow speed and an increase in wave amplitude. Eventually, when the topographic amplitude increases past a critical value, $(h_B)_c$, point C meets point B, and then both solutions terminate. Immediately following the termination the state races toward the other equilibrium state, point A—a catastrophe has occurred.

Immediately after point C meets point B, $D([u])$, which experiences a resonant increase, reduces $[u]$ at an accelerated pace, and the wave amplitude experiences a resonant increase in a positive feedback. As a result, the energy is released from the mean flow to the wave. Thus, the resonance and the positive feedback are the basic cause of the suddenness of SSW. The wave amplitude reaches a peak as $[u]$ becomes zero (Fig. 8). This feature, which appears in the model, is due to the conservation of potential enstrophy. The maximum wave potential vorticity amplitude is achieved when the zonal mean flow potential vorticity becomes zero (Davies, 1981). As $[u]$ turns more easterly, the wave amplitude undergoes a rapid decay. The square of the wave amplitude tends to follow the resonant shape of $D([u])$, though maximum wave amplitude corresponding to zero $[u]$ instead of $[u]_{\text{reso}}$. Subsequently, the further overshooting brings $[u]$ to a maximum easterly and brings about the corresponding warming peak. This description of the evolution of SSW fits very well with observation. A Lagrangian view of the overshooting process leading to the warming peak, after the buildup of the wave, was presented by Matsuno (1983).

As $[u]$ changes from superresonant to subresonant after the instability starts, the phase of the wave changes, according to linear resonance theory, from an in-phase to a 90° out-of-phase (when $[u] = [u]_{\text{reso}}$) then to a greater out-of-phase relationship with respect to the topographic forcing. In the present nonlinear model, similar phase change is followed, though it is not synchronized with $[u]$ in the same manner (Fig. 8). Such a phase change preceding the warming peak corresponds to a westward movement of the wave. Observations (e.g., Quiroz *et al.*, 1975), however, show both eastward and westward movement of thermal centers (and often followed by a poleward movement as the polar region warms up). Such a discrepancy may be attributed to the truncation of the model.

In the HM model, $[u]$ at point A may lie within the range of zonal flow such that the Charney–Drazin criterion is met for most of the model vertical domain, $0 < [u]_A < [u]_{CD}$. In this case, point A is no longer a steady solution (as in a barotropic flow). Instead, due to wave and mean flow interaction point A is replaced by a quasi-periodic solution, V; i.e., a vacillation involving critical level descent as explained by HM and HD. The Charney–Drazin criterion also explains why solution C remains stable when the CD system is replaced by the HM system.

The maximum allowed $[u]_A$ is $[u]_{\text{reso}}$ ($\sim \beta/K^2$, where K is the total wavenumber). Since $[u]_{CD} < [u]_{\text{reso}}$, A, the steady external 180°-out-of-phase solution, can exist in the baroclinic atmosphere, which is the steady state solution we found in experiments with wavenumber 1 when h_B is small; A is also found in some wavenumber 2 experiments with reducing h_B before the transition into solution C.

In the HM model, when $\partial U_R/\partial z$ is reduced, $[u_e]$ is reduced and the line $\kappa([u] - [u_e])$ moves leftward and downward; the critical amplitude $(h_B)_c$ becomes smaller as was obtained in the model experiments (Fig. 10). Such dependence implies that if a SSW has not already occurred, as the season advances from winter solstice to vernal equinox, the chance of an occurrence of a SSW becomes greater and greater. Similarly it is easy to see from Fig. 14 that $(h_B)_0$ should diminish as dU_R/dz is reduced as already shown in Fig. 10. The greater slope of the $(H_B)_0$ curve than that of the $(H_B)_c$ curve in Fig. 10 is related to the fact that $D([u])$ is proportional to the square of topographic amplitude. Thus, Fig. 10 is well explained by Fig. 14. The decrease of $(h_B)_c$ as U_B is decreased, as reported in the last paragraph of Section 4.b, is explained by the fact that $[u_e]$ is reduced by a decreased U_B. Furthermore, the steady state results with wavenumber 1, before its transition into the vacillation regime (Section 4d), correspond to point A in Fig. 14. The failure to obtain the steady state corresponding to C in the wavenumber 1 experiments must be due to the fact that $[u]_{\text{reso}}$ is greater than $[u_e]$ that both B and C do not exist. Indeed, when the experiment was repeated with $\partial U_R/\partial z$ increased to 9 m s^{-1}/km (unrealistically large), a steady state corresponding to point C was found, and when h_B became sufficiently large a qualitatively realistic SSW occurred.

Thus, Fig. 6 does not present a complete picture. A better presentation is given in Fig. 15. Some of the solutions in Fig. 15 may or may not exist and may occupy more or less domain of h_B depending on the model parameters. The thick lines in Fig. 15 represent barotropic solutions; C is the near radiative equilibrium steady solution, which is nearly in-phase with respect to the bottom forcing. If the model is barotropic, solution A′, like A, is stable and steady; both are largely 180° out-of-phase with respect to the bottom forcing. If the model is baroclinic, A′ becomes unstable and new solutions V and V′ associated with the baroclinic modes appear. Solution V is the vacillation regime. The period of vacillation of V increases as h_B decreases and solution V′ is its steady state low forcing limit (solution (b) of Fig. 13), which exhibits similar time mean features as solution V. The transition between V and V′ is a bifurcation.

6. Discussion and conclusion

The repeated warmings in the vacillation regime, as shown in HM, involve a gradual descent of the critical line, and have a period of tens of days; they do not

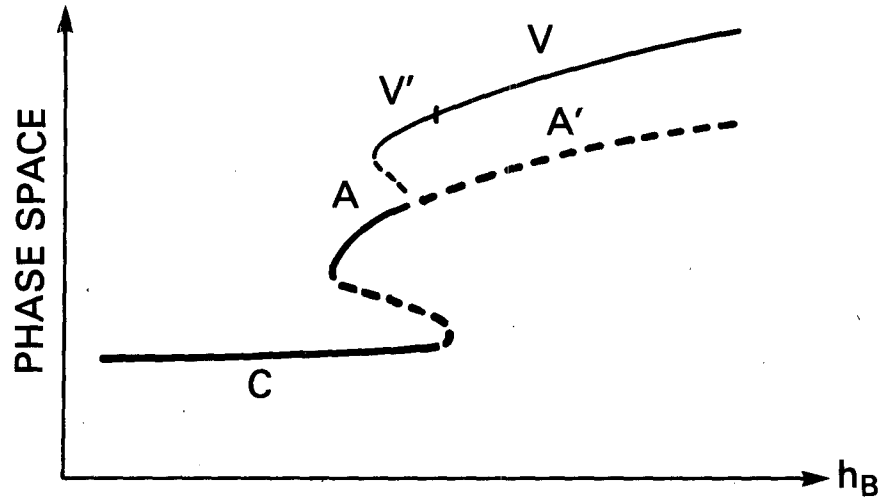

FIG. 15. Schematic representation of solutions in a β-plane channel flow model with one wavenumber and one wave mode. The thick lines represent solutions if the model is barotropic. Solution C is the near radiative equilibrium solution which is nearly in-phase with respect to the bottom wave forcing. Solutions A and A' are the "blocking" solution which is largely 180° out-of-phase with respect to the bottom wave forcing. If the model is baroclinic, A' becomes unstable and new solutions V and V' appear; V is the vacillation solution and V' its steady state limit.

have the explosive characteristics of a real warming. Though interesting theoretically, they do not appear to be relevant in explaining any real phenomena, because before the warming can repeat as described in HM, other important physical processes such as changes in the external forcings and nonlinear interaction among waves of different wavenumbers, preclude the occurrence of such a slow warming. However, the first warming in the HM model (as reported in 4a) involves a catastrophic transition of the flow from a superresonant steady regime to a vacillation regime, and has many characteristics of a real warming, such as the resonant intensification of the planetary wave followed by its rapid decay, and then the reversal of the zonal flow at all levels almost simultaneously and, most importantly, the suddenness of the event [see Fig. 4 of Matsuno (1983) for observational results]. Though a complete description of a real warming should take into account the modifying effects of the nonlinear wave–wave interaction (e.g., Smith, 1983; Austin and Palmer, 1984) and the sphericity, the HM model succeeds in capturing the major physical process of a real warming—a catastrophic flow regime transition.

More general models allowing more meridional modes have generated essentially the same results as HM's model results. The northern and southern wall boundaries in the HM model provide a perfect reflector for the wave and thus facilitate the formation of resonance. In a more realistic description these perfect reflectors should be replaced by partial reflectors. Though resonance can still occur, the required $(h_B)_c$ would be greater. Nevertheless, the conceptual explanation for SSW given in Section 5 still holds. To establish that the onset of SSW in nature is catastrophic, one needs to experiment with an even more general model allowing sphericity and more zonal wavenumbers. One such model (Koermer *et al.*, 1983) has favorably indicated the existence of critical bottom forcing. Furthermore, the observed suddenness of SSW and the rapid return of the westerly strongly suggest that the onset of SSW in nature is catastrophic.

The topographical forcing that we have emphasized in this paper should be considered as the sum of the topographical forcing and the thermal forcing due to the land–sea contrast. The relative importance of the two is a subject of great interest. A recent review of this subject is given by Held (1983).

If a model stratosphere possesses multiple equilibrium states, then no matter how crude the model is, it is possible to generate a sudden warming. This and the near barotropic nature of the SSW explain why some of the early stratospheric models could be used to obtain events qualitatively resembling sudden warmings, despite their crudeness in vertical resolution (e.g., Trenberth, 1973). The necessary criteria for SSW to occur may not always be met in every winter that is modeled. Thus, some general circulation models were able to obtain warmings in some winters, while other winters in the same simulation may have been quiescent (Grose and Haggard, 1981).

The successful forecast of sudden warming events depends very much on the initial conditions. If the initial conditions are (as in the case of beginning the forecast simulation only a few days before the warming peak) such that they represent a point in phase space—in the model as well as in nature—that is, already over the potential energy barrier in a triggered warming case or that has met the instability criteria in a spontaneous warming case, and is already on its way down the new potential energy valley (i.e., the wave amplitude is al-

ready in the accelerated increasing phase), then it is very simple to obtain the warming; however, the success of predicting the intensity and the detailed structure of the warming still depends on the fidelity of the model. An additional and perhaps more difficult challenge in forecasting a triggered SSW comes when the initial conditions represent a point in phase space that has not passed over the potential energy barrier; i.e., the rapid buildup of wave amplitude is not obvious yet, as in the case of starting the forecast simulation far ahead of the real warming. This challenge is twofold. The first is that of correctly simulating the energy barrier, and the second is the challenge of simulating the triggering mechanism. On the other hand, if the warming is spontaneous, the correct forecasting of the growth of forcings external to the stratosphere to meet the instability criterion presents an equally difficult challenge. The high sensitivity of critical forcing amplitude to the external parameters reported in Section 4 indicates the difficulty. A slight imperfection in the model or inferior initial conditions can hasten, delay or even preclude the warming event and make the forecast highly inaccurate, i.e., lower predictability. Thus, there is a significant temporal variation in the stratospheric predictability during the period of onset of sudden warmings.

In attributing SSW to essentially the same instability mechanism that explains blocking (Section 5), we take the view that SSW and tropospheric blocking are different manifestations of an instability process occurring in the troposphere and stratosphere as a whole. This instability occurs frequently and has a range of different zonal wavenumbers. When the stratospheric condition is unfavorable for vertical wave propagation, this instability is confined in the troposphere as a blocking without SSW, as often is the case. With the right zonal wavenumber and when the stratospheric condition (refractive index) is suitable, the resonance cavity, which is usually confined in the troposphere, can extend to the stratosphere and the mesosphere. Thus, the instability can affect the atmosphere from surface to mesopause. This instability, being forced by orography and land–sea thermal contrast, first occurs in the troposphere as blocking and spreads simultaneously into the stratosphere leading to warming. The upward spreading accounts for the fact that blocking occurs slightly before the wave amplitude peaks in the stratosphere. The surge of wave amplitude observed at tropopause level prior to warming is a result of the instability mechanism and thus should not be considered as the initiator of the instability; this is often used as justification for raising the bottom wave forcing amplitude rapidly to initiate SSW in many mechanistic models. Though successful in getting SSW, these mechanistic models obtain rather artificially triggered SSW. Of course, the spontaneous SSW depicted in Section 4a does not represent a precise picture either, because in nature the state is never in an exact equilibrium before SSW. Something like the example given in Section 4c, which requires a light trigger starting from a state close to critical point, is a much better depiction of the real events.

In summary, the current study shows that SSW can be identified as a catastrophic event whose associated instability is the topographically forced Rossby wave instability. The associated multiple equilibria owe their existence to the resonant response to bottom wave forcing. Many of the previous modeling and observational results related to SSW can be interpreted in the light of catastrophe theory. Basic concepts in catastrophe theory related to SSW—hysteresis, cusp, and triggering—are demonstrated in a numerical study using the Holton–Mass model. The chain of events in SSW, the rapid buildup of the planetary wave followed by its quick decay and then by the warming peak, are well explained by the topographically induced Rossby wave instability and are simulated in the HM model. The suddenness of SSW is due to the resonant increase of wave amplitude and its positive feedback on the mean flow. A surge in the wave amplitude at upper tropospheric levels prior to the warming peak is a result of the instability and, as such, should not be used as a trigger to instigate SSW, as is done in many previous mechanistic models. Finally, additional challenge in the SSW forecasting effort comes when the initial conditions have not yet shown any sizable planetary wave amplitude.

Acknowledgments. The author thanks Professor James R. Holton for kindly providing the code listing for the Holton–Mass model for comparison purposes. Thanks are also extended to Professor Akio Arakawa for discussion and to Roberta M. Duffy for typing this manuscript.

REFERENCES

Arnold, V. I., 1984: *Catastrophe Theory* (Translated by R. K. Thomas), Springer-Verlag, 79 pp.

Austin, J., and T. N. Palmer, 1984: The importance of nonlinear wave processes in a quiescent winter stratosphere. *Quart. J. Roy. Meteor. Soc.*, **118**, 289–301.

Buzzi, A., A. Trevisan and A. Speranza, 1984: Instability of a baroclinic flow related to topographic forcing. *J. Atmos. Sci.*, **41**, 637–650.

Charney, J. G., and J. G. DeVore, 1979: Multiple flow equilibria in the atmosphere and blocking. *J. Atmos. Sci.*, **36**, 1205–1216.

——, and D. M. Straus, 1980: Form-drag instability, multiple equilibria and propagating planetary waves in baroclinic, orographically forced, planetary wave systems. *J. Atmos. Sci.*, **37**, 1157–1176.

Davies, H. C., 1981: An interpretation of sudden warmings in terms of potential vorticity. *J. Atmos. Sci.*, **38**, 427–445.

Dutton, J. A., 1982: Fundamental theorems of climate theory—some proved, some conjectured. *SIAM Rev.*, **24**, No. 1, 1–33.

Fultz, D., R. R. Long, G. V. Owens, W. Bohan, R. Kaylor and J. Weil, 1959: Studies of thermal convection in a rotating cylinder with some implications for large scale atmospheric motions. *Studies of Thermal Convection, Meteor. Monogr.*, No. 21, Amer. Meteor. Soc., 104 pp.

Geisler, J. E., 1974: A numerical model of the sudden stratospheric warming mechanism. *J. Geophys. Res.*, **79**, 4989–4999.

Geller, M. A., K. Takano, W. J. Massman, J. E. Rosenfield, W. C. Chao and E. Kalnay, 1985: General circulation modeling of 1979 stratospheric warmings. Submitted to *Mon. Wea. Rev.*

Grose, W. L., and K. V. Haggard, 1981: Numerical simulation of a sudden stratospheric warming with a three-dimensional, spectral, quasi-geostrophic model. *J. Atmos. Sci.*, **38,** 1480–1497.

Held, I. M., 1983: Stationary and quasi-stationary eddies in the extratropical troposphere: theory. *Large-Scale Dynamical Processes in the Atmosphere,* B. J. Hoskins, and R. P. Pearce, Eds., Academic Press, 397 pp.

Hirota, I., and Y. Sato, 1969: Periodic variation of the winter stratospheric circulation and intermittent vertical propagation of planetary waves. *J. Meteor. Soc. Japan,* **47,** 390–402.

Holton, J. R., 1976: A semi-spectral numerical model for wave-mean flow interactions in the stratosphere: Application to sudden stratospheric warmings. *J. Atmos. Sci.*, **33,** 1639–1649.

——, 1980: The dynamics of sudden stratospheric warmings. *Annual Review Earth Planet. Sci.*, **8,** 169–190.

——, and C. Mass, 1976: Stratospheric vacillation cycles. *J. Atmos. Sci.*, **33,** 2218–2225.

——, and T. J. Dunkerton, 1978: On the role of wave transience and dissipation in stratospheric mean flow vacillations. *J. Atmos. Sci.*, **35,** 740–744.

Iooss, G., and D. D. Joseph, 1980: *Elementary Stability and Bifurcation Theory,* Springer-Verlag, 286 pp.

Koermer, J. P., A. Kasahara and S. K. Kao, 1983: Numerical studies of major and minor stratospheric warming caused by orographic forcing. *J. Atmos. Sci.*, **40,** 1552–1570.

Lordi, N. J., A. Kasahara and S. K. Kao, 1980: Numerical simulation of stratospheric sudden warmings with a primitive equation spectral model. *J. Atmos. Sci.*, **37,** 2746–2767.

Mahlman, J. D., and L. J. Umscheid, 1984: Dynamics of the middle atmosphere: Successes and problems of the GFDL "SKYHI" general circulation model, *Dynamics of the Middle Atmosphere,* J. R. Holton and T. Matsuno, Eds., Terra Scientific Pub. Co., Tokyo, 501–526.

Matsuno, T., 1971: A dynamical model of the sudden stratospheric warming. *J. Atmos. Sci.*, **28,** 1479–1494.

——, 1983: Circulation and waves in the middle atmosphere in winter. *Space Sci. Rev.*, **34,** 387–396.

McInturff, R. M., Ed., 1978: Stratospheric warmings: synoptic, dynamic and general-circulation aspects. *NASA Ref. Publ.*, 1017, 174 pp.

McIntyre, M. E., 1982: How well do we understand the dynamics of stratospheric warmings? *J. Meteor. Soc. Japan,* **60,** 37–65.

Miyakoda, K., R. F. Strickler and G. D. Hembree, 1970: Numerical simulation of the breakdown of a polar-night vortex in the stratosphere. *J. Atmos. Sci.*, **27,** 139–154.

O'Neill, A., and B. F. Taylor, 1979: A study of major stratospheric warming of 1976–1977. *Quart. J. Roy. Meteor. Soc.*, **105,** 71–92.

Palmer, T. N., 1981: Diagnostic study of a wavenumber-2 stratospheric sudden warming in a transformed Eulerian-mean formalism. *J. Atmos. Sci.*, **38,** 844–855.

Pedlosky, J., 1981: Resonant topographic waves in barotropic and baroclinic flows. *J. Atmos. Sci.*, **38,** 2626–2641.

Plumb, R. A., 1981a: Forced waves in a baroclinic shear flow. Part 2: Damped and undamped response to weak near-resonant forcing. *J. Atmos. Sci.*, **38,** 1856–1869.

——, 1981b: Instability of the distorted polar night vortex: A theory of stratospheric warmings. *J. Atmos. Sci.*, **38,** 2514–2531.

Poston, T., and I. N. Stewart, 1978: *Catastrophe Theory and its Applications,* London, Pitman, 491 pp.

Quiroz, R. S., A. J. Miller and R. M. Nagatani, 1975: A comparison of observed and simulated properties of sudden stratospheric warmings. *J. Atmos. Sci.*, **32,** 1723–1736.

Revell, M. J., and B. J. Hoskins, 1984: Orographically induced Rossby wave instabilities. *J. Atmos. Sci.*, **41,** 51–67.

Saunders, P. T., 1980: *An Introduction to Catastrophe Theory,* Cambridge University Press, 144 pp.

Schoeberl, M. R., 1978: Stratospheric warmings: Observations and theory. *Rev. Geophys. Space Phys.*, **16,** 521–538.

——, 1983: A study of stratospheric vacillations and sudden warmings on a β-plane. Part I: Single wave-mean flow interaction. *J. Atmos. Sci.*, **40,** 769–787.

——, and D. F. Strobel, 1980: Numerical simulation of sudden stratospheric warmings. *J. Atmos. Sci.*, **37,** 214–236.

Simmons, A. J., and R. Strüfing, 1983: Numerical forecasts of stratospheric warming events using a model with a hybrid vertical coordinate. *Quart. J. Roy. Meteor. Soc.*, **109,** 81–111.

Smith, A. K., 1983: Observation of wave–wave interactions in the stratosphere. *J. Atmos. Sci.*, **40,** 2484–2496.

Sturrock, P. A., 1966: Explosive and nonexplosive onsets of instability. *Phys. Rev. Lett.*, **16,** 270–273.

Thom, R., 1972: *Structural Stability and Morphogenesis,* (English translation by D. H. Fowler, 1975), Benjamin, Reading, Mass.

Trenberth, K. E., 1973: Dynamic coupling of the stratosphere with the troposphere and sudden stratospheric warmings. *Mon. Wea. Rev.*, **101,** 306–322.

Vickroy, J. G., and J. A. Dutton, 1979: Bifurcation and catastrophe in a simple, forced, dissipative quasi-geostrophic flow. *J. Atmos. Sci.*, **36,** 42–56.